SEMARAK ILMU PUBLISHING

Journal of Advanced Research in Fluid Mechanics and Thermal Sciences

Journal homepage:
https://semarakilmu.com.my/journals/index.php/fluid_mechanics_thermal_sciences/index
ISSN: 2289-7879

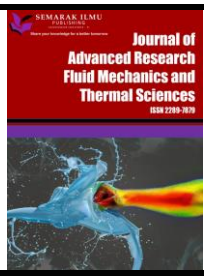

Effect of Indentation at Rolling Body Surfaces on the Film Formation in Elastohydrodynamic Lubrication Contact under Dynamic Loads

Dedi Rosa Putra Cupu[1], Kahar Osman[2], Zulhanafi Paiman[2,*]

[1] Department of Mechanical Engineering, Faculty of Engineering, Universitas Riau, 28293 Pekanbaru, Riau, Indonesia
[2] Department of Mechanical Engineering, Fakulti Kejuruteraan Mekanikan, Universiti Teknologi Malaysia, 81310 Skudai, Johor, Malaysia

ARTICLE INFO

Article history:
Received 15 December 2023
Received in revised form 27 April 2024
Accepted 13 May 2024
Available online 30 May 2024

Keywords:
Elastohydrodynamic lubrication; EHL point contact; sinusoidal dynamic load; artificial indentation

ABSTRACT

Vibration is one of the phenomena that can occur during the operation of roller bearing which can lead to dynamic loads being subjected to the contact and thus, affect the film formation in elastohydrodynamic (EHD) contacts. On the other hand, surface textures such as artificial indentations and grooves greatly affect the film formation as well as the corresponding pressure distribution in the contact area, since the depths of the textures are usually much greater than the film thickness in the contact. This paper investigates the influence of an artificial indentation located on the rolling element, which passes through a point contact under dynamic loads by means of numerical simulations. Solutions to the Reynolds equation are performed and calculations of the elastic deformation equation, force balance equation and lubricant properties equations to show the effects of both indentation passing through the contact and a sinusoidal dynamic load on the film thickness as well as pressure profile of EHD point contact. Moreover, the effect of frequency and amplitude excitation of the dynamic load on the film formation was investigated. The results revealed that the artificial indentation under sinusoidal dynamic load of EHD point contact induced a significant effect on the thickness of the film formation and pressure distribution.

1. Introduction

A study of contact between machine elements such as journal bearings, gears, rolling element bearings as well as cams and followers can be simply analyzed as a contact model between two solid bodies contacting each other with relative motion and the contact is subjected to external load [1-3]. This contact generates very high pressure over a very small localized contact area. In the case of cylindrical rolling element bearing application, the contact between cylindrical roller element and raceway is often modelled as a line contact between a solid cylinder and a flat plate [2]. For ball bearing application, the contact is modelled as a point contact of spherical ball and flat plate [3]. The first period of EHL point contact analyses, simulations were performed under steady operating conditions, in which the contacting surfaces were assumed to be perfectly smooth, and the operating

* *Corresponding author.*
E-mail address: zulhanafi.paiman@utm.my

https://doi.org/10.37934/arfmts.117.2.157171

conditions such as the applied load, the entrainment velocity, and Hertzian radii were constant. This simulation situation was studied by Dowson and Higginson [4], Hamrock and Dowson [5-8], Evans and Snidle [9]. Then, in the last three decades, the great development of EHL point contact simulation has been significantly improved in terms of calculation times and stability by introducing a multigrid method as conducted by Lubrecht [10], a multilevel integration technique by Brand and Lubrecht [11], and a distributive relaxation technique by Venner [12] as well as a progressive mesh densification as introduced by Zhu [13]. These numerical results have then been confirmed by experimental investigations using optical interferometry concept and Spacer Layer Imaging Method [14-16].

In recent years, modern design of heavy-duty mechanical systems requires machine elements to work under high-load conditions. This causes the thickness of the lubricant film formation to decrease down to be hundreds of nanometers. On the other side, a presence of inevitable vibrations during operation of ball bearing, especially due to high-speed operation, induces a change in the external load applied to the contact. The high amplitude of vibration excitation increases the applied load and decreases the thickness of the lubricant film formation [17]. If the film is tiny, asperities of the rough surfaces will be in contact and thus, lead to sudden or unexpected bearing failure due to wear [18]. However, studies carried out by researchers have shown, that artificial modified surface textures, such as indentations and grooves, give a promising approach to increase the film thickness [19-22]. In the past four decades, the situations of the surface textured contacts under static applied loads have been investigated experimentally and numerically [23-27].

With respect to point contact EHL under sinusoidal dynamic loads, Wijnant and Venner [28] found that the inertia forces of ball bearing caused the contact force variation and thus the film thickness and pressure varied in the contact area. In addition, Wijnant [17] numerically studied the effects of external sinusoidally dynamic load to observe the stiffness and damping in a single EHL point contact. He also investigated the effects of sinusoidally varying loads on the film formation and pressure distribution generated in the EHL point contact. It was shown, that the sinusoidal dynamic loads altered the contact area. This increased and decreased the film formation cyclically. Moreover, it was also shown that wavelength modulations increased with increasing frequency excitation subjected to the contact. These numerical results from Wijnant [17] were then proved experimentally by Wijnant *et al.,* [29] who carried on a ball-on-disc tribometer to observe the effect of impact load on the interferometric lubricant film thickness. Furthermore, El Kilali *et al.,* [30] developed a new experimental apparatus using optical interferometry technique to simultaneously measure the change of the lubricant film thickness due to a free shock of load subjected to the elastohydrodynamic contact at constant rolling speed. Sakamoto *et al.,* [31] also conducted an interferometric-based experiment to investigate the effects of cyclic pulsating and impact loads on film thickness of EHL point contact. Later, Glovnea and Zhang [32] numerically and experimentally studied the effect of the periodic load variation on the film thickness distribution. The results from El Kilali *et al.,* [30], Sakamoto *et al.,* [31], and Glovnea and Zhang [32] were similar, in which there were film thickness perturbations on the contact area due to the quick changes of the load over time. The increase or decrease of the load quickly led to a larger or smaller contact area creating a local reduction or expansion in the film thickness formation. Glovnea and Zhang [32] also showed that the contact area was directly affected by the load variation. It is noted that the forces due to inertia in the lubricant were negligibly small compared to the viscous forces because the film thickness between the contacting surfaces was relatively small compared to the contact area. This caused the Navier-Stokes equation was reduced to an equation of the generated pressure in the gap of the contacing surfaces, namely the Reynolds equation. However, the neglecting forces in the Wijnant's

work probably can be determined by the so-called CFD method as studied by previous researchers [33,34].

From the above-mentioned studies, it can be concluded that the artificial indentations can be used to improve the thickness of the film formation. However, the studies of the artificial indentation were confined exclusively to the static load. Meanwhile, other studies related to the dynamic loads were restricted to the smooth contacting surfaces, which mean the effects of the surface features were neglected. Hence, the aim of the present study is to investigate the combination of both effects of dynamic loads and artificial indentation on the behavior EHL point contact under pure rolling conditions by means of numerical simulations.

2. Methodology

2.1 Model Formulation

Figure 1 shows a contact between a single ball element bearing and its raceway can be mathematically modeled as a contact between a spherical roller and an infinite flat plate which is referred to as EHL point contact [35]. Studying EHL problems means solving a number of equations: the Reynolds equation, the elastic deformation equation, the force balance equation and lubricant properties equations. Under isothermal conditions, the Reynolds equation for the transient point contact problem stated in dimensionless form as introduced by Reynolds [36]

$$\frac{\partial}{\partial X}\left(\xi\frac{\partial P}{\partial X}\right)+\frac{\partial}{\partial Y}\left(\xi\frac{\partial P}{\partial Y}\right)-\frac{\partial(\bar{\rho}H)}{\partial X}-\frac{\partial(\bar{\rho}H)}{\partial T}=0 \tag{1}$$

All dimensionless variables are defined in the nomenclature. The boundary conditions are $P(X_a,Y,T)=P(X_b,Y,T)=P(X,Y_a,T)=P(X,Y_b,T)=0$. X_a, X_b, Y_a and Y_b refer to the boundaries of the entire domain. In this study, rolling and sliding motions take place in the X direction, while the Y direction is perpendicular to rolling direction. Furthermore, the cavitation condition in the Reynolds equation must be satisfied at all times $(P(X,Y,T)\geq 0)$, ξ is defined as

$$\xi=\frac{\bar{\rho}(X,Y,T)\cdot H(X,Y,T)^3}{\bar{\eta}(X,Y,T)\bar{\lambda}} \tag{2}$$

where

$$\bar{\lambda}=\frac{12u_m\eta_0R_x^2}{a^3p_h} \tag{3}$$

The pressure-viscosity equation proposed by Roelands [37] and the pressure-density relation from Dowson and Higginson [4] are adopted in this simulation.

$$\bar{\eta}_{i,j}=e^{\left\{\frac{\alpha p_0}{z}\left[-1+\left(1+\frac{p_hP_{i,j}}{p_0}\right)^z\right]\right\}} \tag{4}$$

$$\bar{\rho}_{i,j}=\frac{0.59\times10^9+1.34p_hP_{i,j}}{0.59\times10^9+p_hP_{i,j}} \tag{5}$$

The dimensionless film thickness between two contacting surfaces by accounting the indentation on one surface can be expressed as

$$H(X,Y,T) = H_0(T) + \frac{X^2}{2} + \frac{Y^2}{2} + C_{(X,Y,X',Y')}P(X',Y',T) - \bar{R}(X,Y,T) \quad (6)$$

$H_0(T)$ corresponds to the integration constant determined by the force balance condition and $\bar{R}(X,Y,T)$ denotes the undeformed geometry of the indentation at dimensionless time T. Indentation is assumed to be located on the ball moving with the velocity u_2 (upper surface velocity) and can be modeled in dimensionless form as

$$\bar{R}(X,Y,T) = \bar{r}(x,y,t)R_x/a^2 \quad (7)$$

$\bar{r}(x,y,t)$ is the indentation geometry that used by Coulon *et al.,* [38] and can be read as

$$\bar{r}(x,y,t) = d_{th}e^{\left(-K\frac{(x-x_d)^2+y^2}{4\emptyset^2}\right)}cos\left(\frac{\pi\sqrt{(x-x_d)^2+y^2}}{\emptyset}\right) \quad (8)$$

where d_{th} and $\emptyset$ denote the depth and the diameter of the indentation, respectively whereas *K* refers to shoulder's height factor and x_d is the position of the indentation: $x_d = x_s + u_2t$ denotes the position of the indentation at $t = 0$. In dimensionless form, the position of the indentation reads

$$X_d = x_d/a \quad (9)$$

$C_{(X,Y,X',Y')}$ in Eq. (6) represents the influence matrix of the deformation (X',Y') describing the influence of the pressure *P* on the displacement of the point at location of (X,Y). Singularity occurs at $X = X'$ and $Y = Y'$ which can be solved by adopting the equal pressure across the rectangular surface into a matrix of influence coefficients. The influence matrix of $C_{(X,Y,X',Y')}$ is then simply solved analytically by Love [39].

By accounting for the external sinusoidal dynamic load, the dimensionless force balance equation as mentioned by Wijnant [17] reads

$$\int_{-\infty}^{\infty}\int_{-\infty}^{\infty}P(X,Y,T)dXdY = \frac{2\pi}{3}(1 + \bar{A}\,sin(\Omega_eT)) \quad (10)$$

where $\bar{A}$ denotes the oscillation amplitude of the vibration and Ω_e is its excitation frequency.

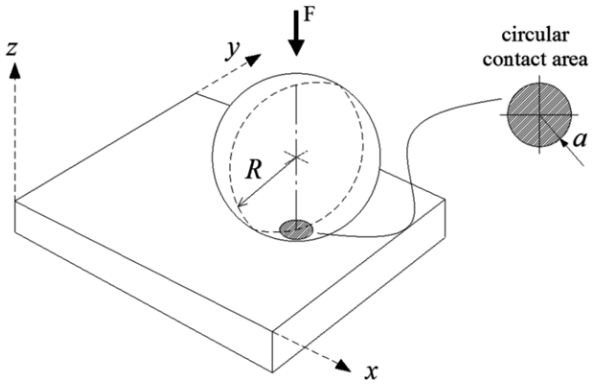

Fig. 1. Simplification of spherical ball and infinite flat plate contact problem [35]

2.2 Numerical Procedure

To solve the EHL point contact problems, the finite difference method was used to solve the Reynolds equation. First, the system equations were discretized on a uniform grid with mesh size h in X and Y direction. The discretization process covered a set of points inside a rectangular domain of $X\_a \leq X \leq X\_b, -Y\_a \leq Y \leq Y\_b$ which represented a regularly spaced mesh of $(M\ x\ N)$. The Reynolds equation was solved using Jacobi relaxation with single grid solution, while the elastic deformation equation was solved using half-space theory at each time step. By setting the equidistant grids of X and Y direction $(\Delta X = \Delta Y)$, the discretization of Reynolds equation, the dimensionless film thickness, the dimensionless viscosity and density as well as the force balance equation followed the previous study [40].

Figure 2 shows the flowchart of transient EHL point contact problem simulation in this study. The results from the previous time step were used to perform the current time step simulation. The numerical technique was performed at each time step was similar to that for a stationary solution. The calculations were simulated on the domain of $-2.5 \leq X \leq 1.5$ and $-2.0 \leq Y \leq 2.0$ with 129*129 grid points. This corresponded to a mesh size of $\Delta X = \Delta Y = 0.03125$. The time increment was set equal to the mesh size $\Delta T = \Delta X = 0.03125$. The simulation was started with the location of the indentation at $X\_s = X\_d\ (T = 0) = -2.5$. This choice ensured that there were no numerical start-up effects when the indentation started affecting the EHL behavior [26,27]. However, the contact has been subjected to the sinusoidal dynamic load started from the second time step and so on, this followed the numerical methods conducted by Cupu *et al.,* [41] for the case of smooth EHL point contact under sinusoidal dynamic loads.

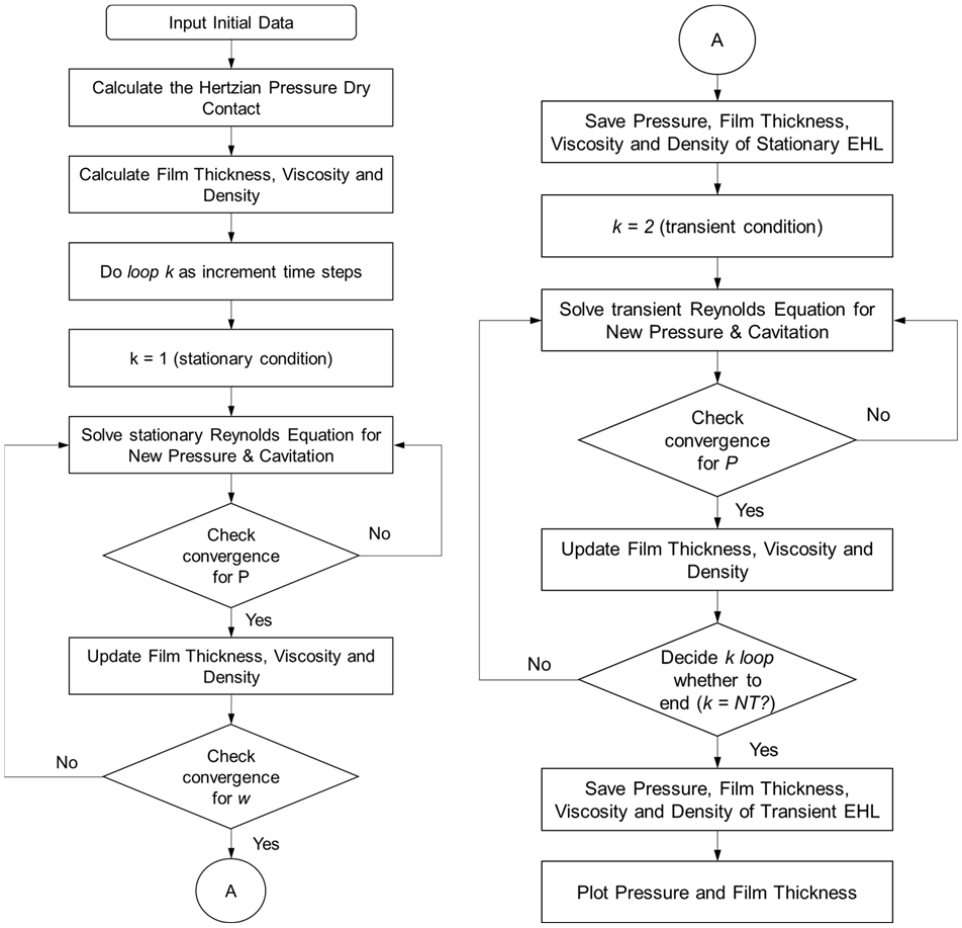

Fig. 2. Flow chart of the transient EHL Point Contact

3. Results and Discussion

3.1 Pressure Distribution

The primary objective of this paper is focused on the EHL behavior of a moving indentation passing through the EHL point contact subjected to the sinusoidal dynamic loads under pure rolling condition. This means that the speeds of two contacting surfaces are equal (slide-to-roll ratio, SRR = 0). The spherical ball is indented using Eq. (8) with a diameter of 0.1 mm and depth of 0.1 µm, as shown in Figure 3. The operating conditions and some dimensionless parameters used in this paper are referred to the parameter values as shown in previous work by Venner and Lubrecht [27] as listed in Table 1. Under stationary condition, the results of the minimum and central film thickness from the present code are 0.205 and 0.409 µm, respectively. Comparing to the result from Venner and Lubrecht [27] in which the minimum and central film thickness were 0.21 and 0.40 µm, its agreement is very good.

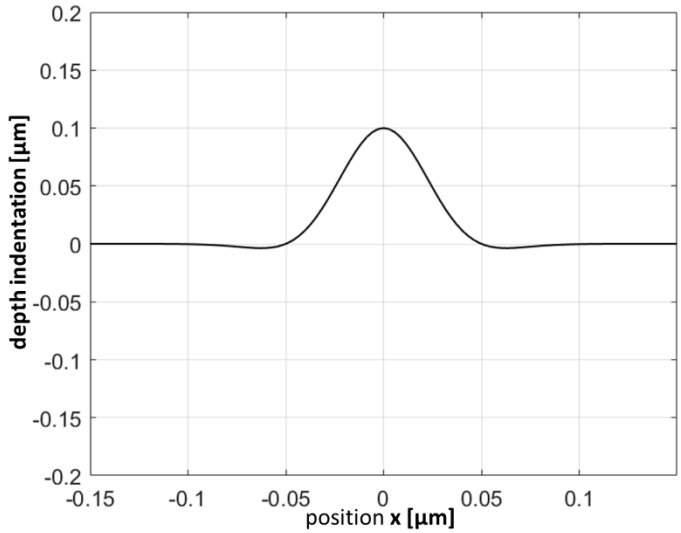

Fig. 3. Cross-section of indentation geometry

Table 1
Parameters and their values for presented condition [26]

Parameter	Value	Dimension
E'	$1.17 \cdot 10^{11}$	[Pa]
α	$2.2 \cdot 10^{-8}$	[Pa^{-1}]
η_0	1.22	[Pa.s]
u_s	$9.6 \cdot 10^{-2}$	[m/s]
R	$1.27 \cdot 10^{-2}$	[m]
a	$1.84 \cdot 10^{-4}$	[m]
p_h	$0.54 \cdot 10^{9}$	[Pa]
Dimensionless parameters		
M	77	-
L	7.9	-
λ	$3.4 \cdot 10^{-2}$	-
W	$2.0 \cdot 10^{-6}$	-
U	$3.9 \cdot 10^{-11}$	-
G	$2.63 \cdot 10^{3}$	-

3.2 Smooth Surface under Sinusoidal Dynamic Load

In order to show the effect of the sinusoidal dynamic loads on the film thickness and pressure profile, simulations were performed for the smooth contacting surfaces with varying oscillation parameters. First, the present code was compared to the result calculated by Wijnant [17], simulation has been performed under conditions identical to those used in his calculation. Wijnant solved a smooth surface EHL point contact under sinusoidal dynamic load of $\bar{A}$ = 0.1 and Ω_e = 2π using multigrid solution with 257*257 grid points at the finest level whereas the present study solves the same problem using single grid method with 129*129 grid points. Figure 4 shows that as the load increased after T = 0, an increase in the pressure profile can be observed in the contact area at T = 0.25 and the pressure decreases and coincides with the previous condition since the load is equal to the condition at T = 0. In this period, the sinusoidal dynamic load has not affected the film thickness. Figure 4 also shows the solution is periodic after $T \geq 2$ every dimensionless time unit, the solution at T = 2 is coincident with that of at T = 3 and so on. The pressure distribution and film thickness profile resulted from the present code give a good agreement with those by Wijnant [17].

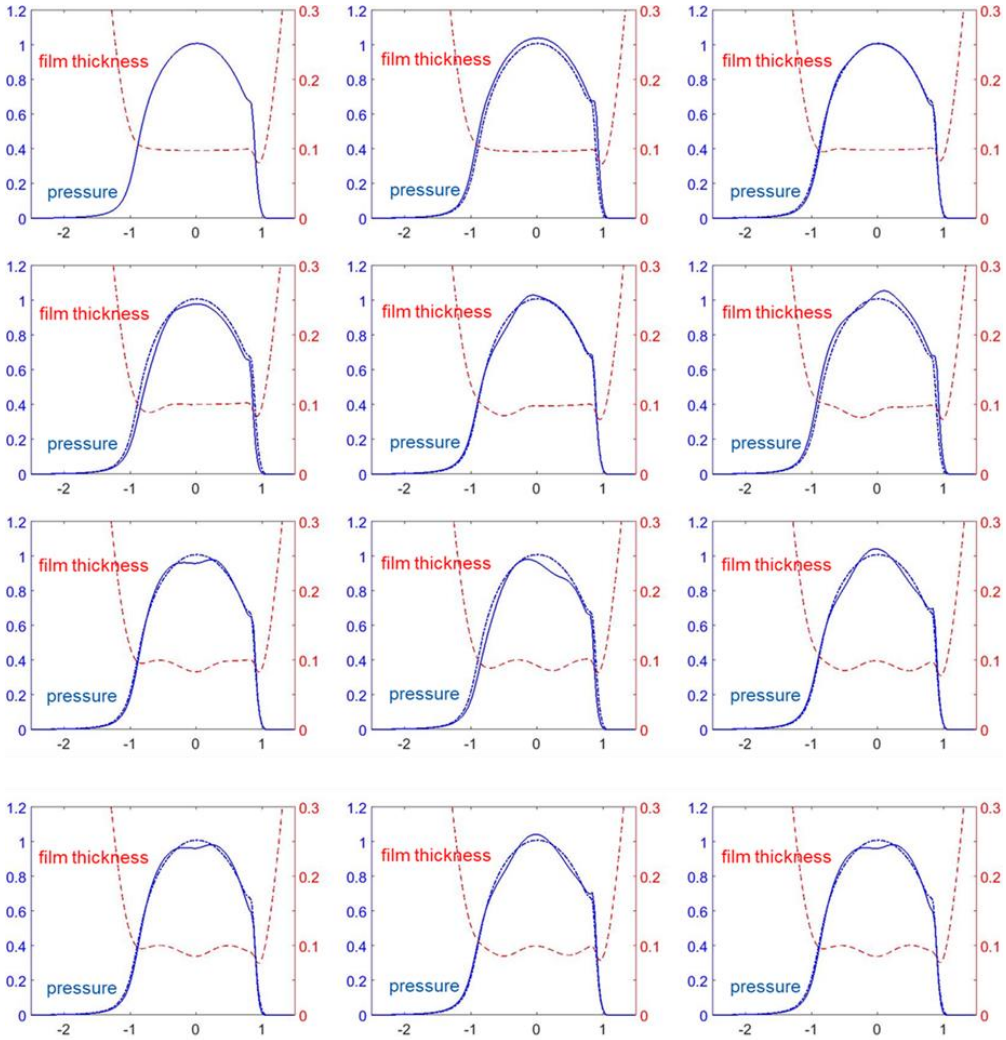

Fig. 4. Centre line pressure (left labels) and film thickness (right labels) for *M* = 100, *L* = 5 and Ω_e = 2π at dimensionless times of *T* = 0, 0.25, 0.5, 0.75, 1.0, 1.25, 1.5, 1.75, 2.0, 2.5, 3.0 and 3.5. The center line pressure is included as a reference by the dotted-dashed line

The effect of the sinusoidal dynamic loads on the pressure and film thickness profile is shown in Figure 5, in which the simulations were performed under different frequency excitation of Ω_e = π and Ω_e = 2π with the same of amplitude excitation of $\bar{A}$ = 0.1. These excitations caused a maximum Hertzian pressure variation of between 0.521 and 0.557 GPa. Figure 5(a) shows the variations over two periods of central and minimum film thickness for the smaller frequency excitation. It can be seen that the increase rate of central film thickness at the maximum load is about 7.88 % and at the minimum load is 5.74 %. In case of the minimum film thickness, the increase rate is about 11.9 % and 7.24 % for maximum and minimum increase compared to the stationary central and minimum film thickness. For the frequency excitation of Ω_e = 2π, the increase rates of the central and minimum film thickness are slightly increase compared to the effect of dimensionless excitation frequency, Ω_e = π, as seen in Figure 5(b). For the excitation of Ω_e = 2π, the central film thickness increases about 8.68 % when the load was maximal and decreases about 8.15 % when the load was minimal. In addition to this observation with respect to the sinusoidally varying loads, other interesting effect shows up when comparing the film thickness and pressure profile at each time step. Since the applied load fluctuated sinusoidally, the changes in film thickness as well as pressure profile became periodic. This means that, the solution results in the similar pressure and film thickness profile after a certain period of time. In this case, the periodicity starts after the changes in the film thickness have spread through the contact, i.e., the periodicity starts after T≥ 2 (t = 7.667 ms). This is in line with the results shown in the literature by Wijnant [17].

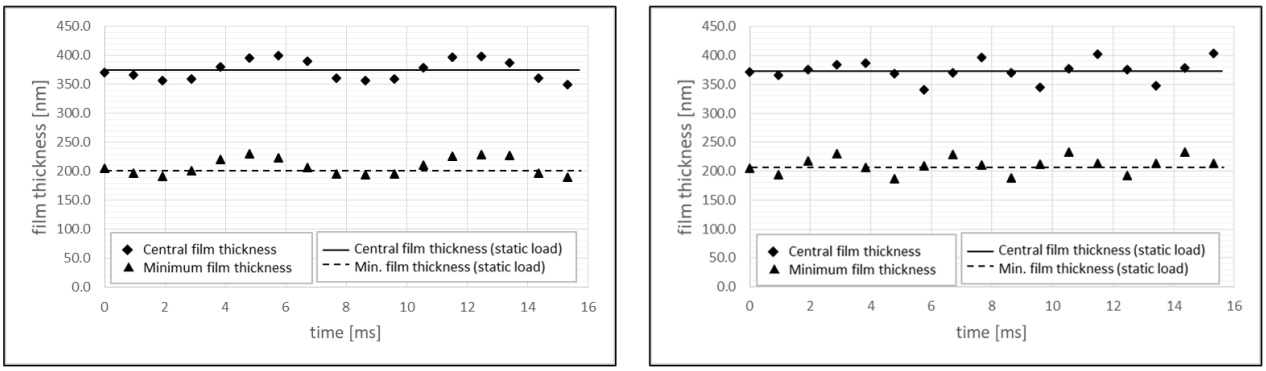

Fig. 5. Central and minimum film thickness profile for different frequency excitation of (a) Ω_e = π and (b) Ω_e = 2π with the same amplitude excitation of $\bar{A}$ = 0.1

The modulations on the film thickness and pressure are more pronounced for the higher frequency excitations. This, for example, can be clearly observed in Figure 5. In this simulation result, the dimensionless excitation frequency was Ω_e = 2π with the same $\bar{A}$ = 0.1. However, the increase rates of the central and minimum film thickness are slightly increase compared to the effect of dimensionless excitation frequency, Ω_e = π, as seen in Figure 5. For the excitation of Ω_e = 2π, the central film thickness increases about 8.68 % when the load was maximal and decreases about 8.15 % when the load was minimal. In addition to this observation with respect to the sinusoidally varying loads, another interesting effect shows up when comparing the film thickness and pressure profile at each time step. Since the applied load fluctuates sinusoidally, the changes in film thickness as well as pressure profile become periodic. This means that the solution results in the similar pressure and film thickness profile after a certain period of time. In this case, the periodicity starts after the changes in the film thickness have spread through the contact, i.e., the periodicity starts after T≥ 2 (t = 7.667 ms). For example, as seen in Figure 5, the film thickness and pressure profile at T = 2 (t = 7.667 ms), see Figure 5(f) are similar to those of at T = 3 (t = 11.380 ms) and T = 4 (t = 15.333 ms), as seen in

Figure 5(g) and Figure 5(j), respectively and so do the film thickness and pressure profile at T = 2.5 (t = 8.505 ms) as seen in Figure 5(g) are similar to those of at T = 3.5 (t = 12.338 ms) in Figure 5(i). This theory is in line with the results obtained by Wijnant [17].

Subsequently, to show the effect of the dimensionless oscillation amplitude on the film thickness and pressure profile more clearly, simulations were performed for different dimensionless oscillation amplitude of $\bar{A}$ = 0.2 and 0.5 with the same frequency excitation of Ω_e = 2π and compared with the previous one. Figure 6 shows the variations in the centerline film thickness and pressure profile at momentarily time of t = 0.838 ms, 3.713 ms and 7.667 ms for $\bar{A}$ = 0.1, 0.2 and 0.5, respectively. The central and minimum film thickness during the sinusoidal dynamic load passing the contact can be seen in Figure 7. As seen in this figure, lower dimensionless amplitude excitation implies relatively small rate of variation of both central and minimum film thickness. At higher dimensionless amplitude excitation, especially at $\bar{A}$ = 0.5, pronounced deviations of film thickness from the lower amplitude can be observed, which leads to increase about 25% and 20% larger, than the lower amplitude excitation values for the central and minimum film thickness, respectively.

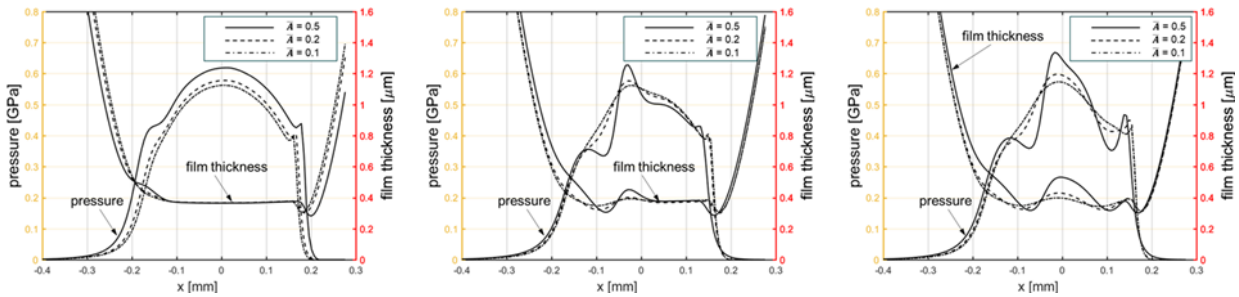

(a) (b) (c)

Fig. 6. Pressure and film thickness profile for $\bar{A}$ = 0.1, 0.2 and 0.5 with Ω_e = 2π at (a) t = 0.838 ms, (b) t = 3.713 ms and (c) t = 7.667 ms

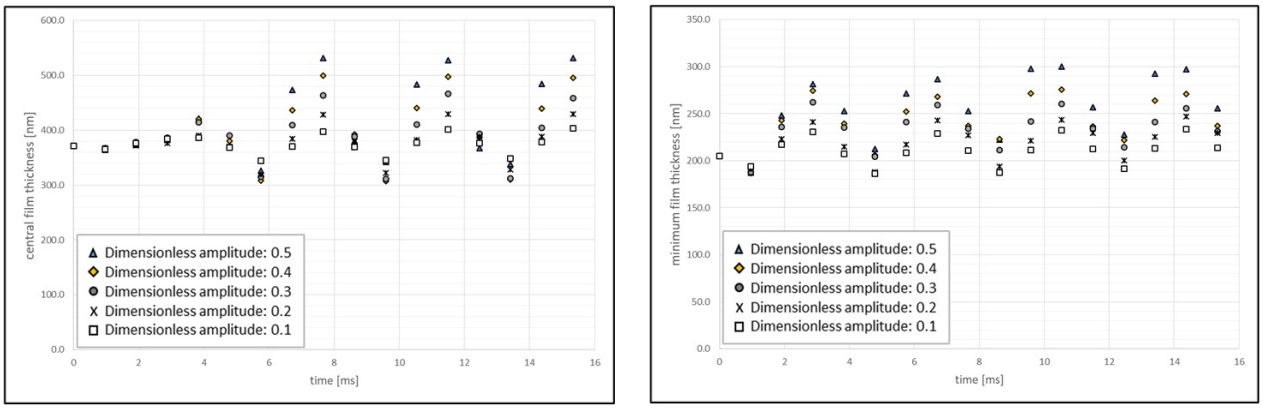

(a) (b)

Fig. 7. Central (a) and minimum (b) film thickness for different dimensionless amplitude excitation for Ω_e = 2π

Furthermore, similar to the results from the low oscillation amplitude, $\bar{A}$ = 0.1 for frequency excitation of 2π as shown in Figure 5(b), the rate modulation of changes in the film thickness and pressure profile periodically occurs every one-time unit which starts after T≥ 2. However, for this particular case, the modulations on pressure and film thickness clearly show up. It should be noted that the increase in pressure as the load increased at the maximum value, i.e., at T = 0.25 (t = 0.838 ms), is very small compared to the situations in which the oscillation amplitudes are higher. For $\bar{A}$ = 0.1, the increased load induces the maximum pressure increased from 0.546 GPa at t = 0 (static load

condition) to 0.561 GPa at t = 0.838 ms (dynamic load condition when the load reaches maximal) whereas for $\bar{A}$ = 0.5, the maximum pressure increase caused by the load variation was from 0.546 GPa at t = 0 to 0.618 GPa at t = 0.838 ms, as shown in Figure 6.

3.3 Indented Surface under Sinusoidal Dynamic Load

Finally, the combined effects of sinusoidally changes in load applying to the contact and indentation on one contacting surface passing through the contact are now considered. Indentation with diameter of 0.1 mm and 0.5 μm of depth is placed on the surface, and a sinusoidal dynamic load is applied to the contact under pure rolling condition. The indentation is first located far away from the high-pressure region, i.e., X_d = -2.5 and initial static load subjected to the contact. Then, a sinusoidal change of load with an oscillation amplitude of 0.1 and frequency excitation of 2π is applied.

Figure 8 displays 12 snapshots of dimensionless pressure and film thickness for indentation with a depth of 0.5 μm. The plots captured the situation when the indentation is placed momentarily at outside and inside the contact area from X_d = -2.5 to X_d = 1.25. It can be seen that, when the indentation is still outside the contact area, i.e., X_d = -1.5, there is only sinusoidal dynamic load effect exists on the EHL behavior, and hence the results must coincide with the smooth contact situation under sinusoidal dynamic load. Then, in few next time step units, the indentation starts affecting the film thickness formation as well as the pressure profile in the contact area along with the sinusoidal dynamic load. Again, since the indentation travels through the contact at the same speed with the average surface velocity, the indentation induces changes in film thickness and pressure profile are localized at the vicinity of the indentation. However, it is interesting to be observed that the periodicity effect of sinusoidal dynamic load is no longer existent due to the effect of the indentation, which means that the pressure profile and film thickness formation are not similar after a certain period of time.

The influence of the indentation depth on the film thickness and pressure profile under pure rolling condition of EHL point contact subjected to the sinusoidally varying load is shown in Figure 9, which shows the central and minimum film thickness during the indentation passing through the contact for different depth of indentation. It can be observed that the central film thickness increases about fifty percent for the indentation depth of 0.5 μm at the center of the indentation, compared to the contact without indentation. For the indentation depth of 0.1 μm and 0.2 μm, the film thickness increases about 17 and 28 percent, respectively. It can also be found from Figure 9(a) that indentation causes a slight increase of the film thickness at the leading edge of the indentation. Noted that the trailing edge is the last portion of the indentation to enter the contact area and the first portion to enter the contact is referred to as the leading edge [42]. Take the indentation with 0.5 μm depth for example, the film thickness increases at the leading edge is only about seven percent. This is because the contact was simulated under pure rolling condition (SRR = 0) so that both two contacting surfaces run with the same velocity. Profound literature study mentioned that the presence of the sliding motion causes the elongation of film thickness enhancement is not only at the indentation, but also spreads downstream or upstream in sliding direction within the contact [16]. However, indentation also induces a significant decrease at the trailing edge. From Figure 9(a), it can be seen that the central film thickness decreases from 369.4 nm to 358.2 nm, 334.2 nm and 299.1 nm due to indentation with the depth of 0.1 μm, 0.2 μm and 0.5 μm, respectively. Nevertheless, since the ball surface was indented at the center of the contact, it does not give any effect on the minimum film thickness, as found from Figure 9(b). As it is known that for the case of EHL point

contacts, the minimum film thickness occurs not at the centerline of the contact, but at each of the two sidelobes.

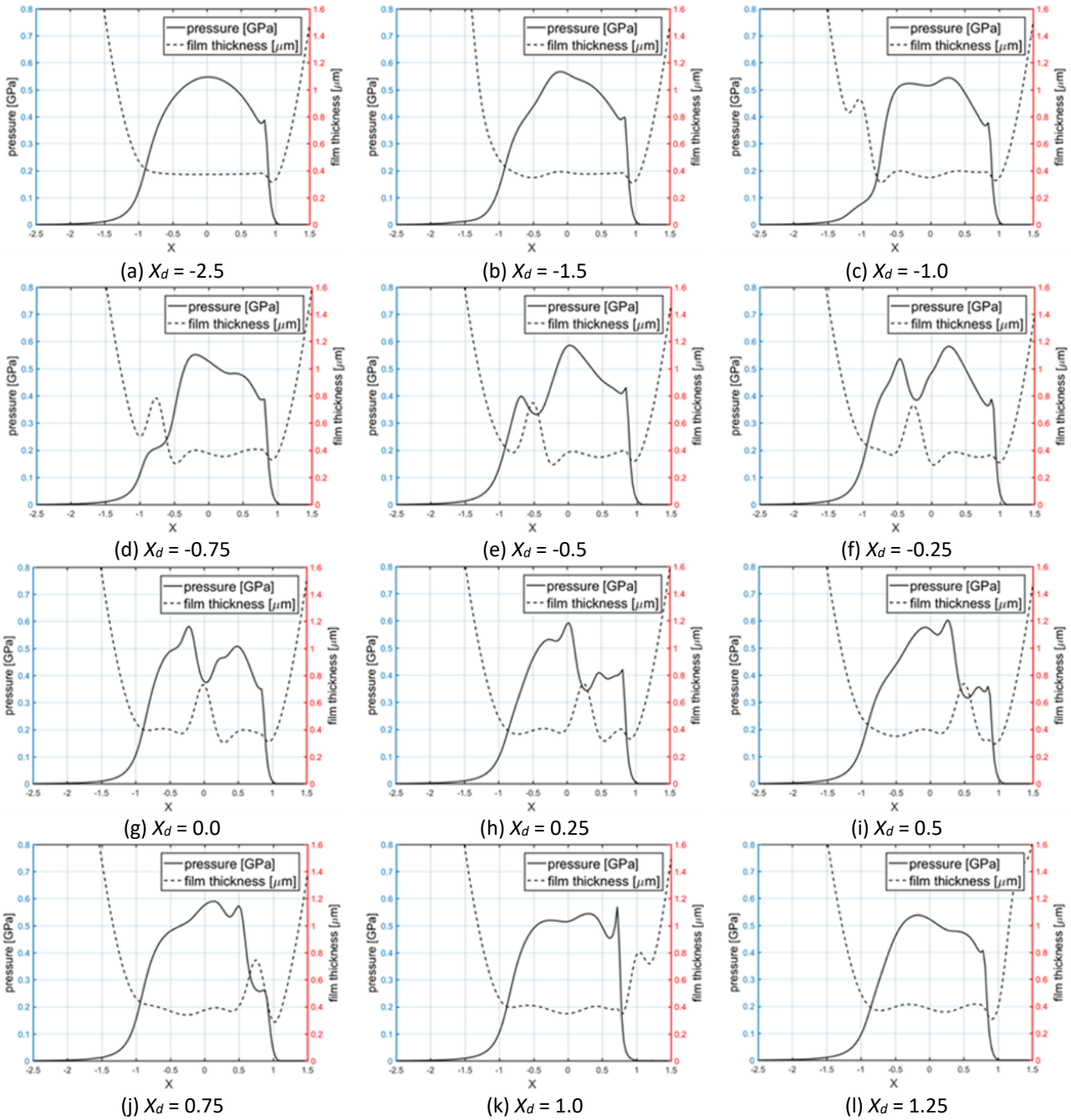

(a) X_d = -2.5 (b) X_d = -1.5 (c) X_d = -1.0

(d) X_d = -0.75 (e) X_d = -0.5 (f) X_d = -0.25

(g) X_d = 0.0 (h) X_d = 0.25 (i) X_d = 0.5

(j) X_d = 0.75 (k) X_d = 1.0 (l) X_d = 1.25

Fig. 8. Transient pressure (left labels) and film thickness (right labels) for indentation with diameter of 0.1 mm and depth of 0.5 µm subjected to dynamic load under pure rolling condition

Subsequently, to compare the effect of the indentation moving into the contact area, Figure 10 shows the plots of film thickness profile for the two conditions of indented contacting surface under static and dynamic load. In this simulation, the upper contacting surface was indented with diameter of 0.1 mm and 0.1 µm depth whereas the parameters of dynamic load were Ω_e = 2π and $\bar{A}$ = 0.1. The location of the indentation is momentarily at the center of the contact, i.e., X_d = 0. From Figure 10, it can be observed that the indentation increases the film thickness at the vicinity of the indentation. However, the edge of the indentation caused a small decrease in film thickness distribution.

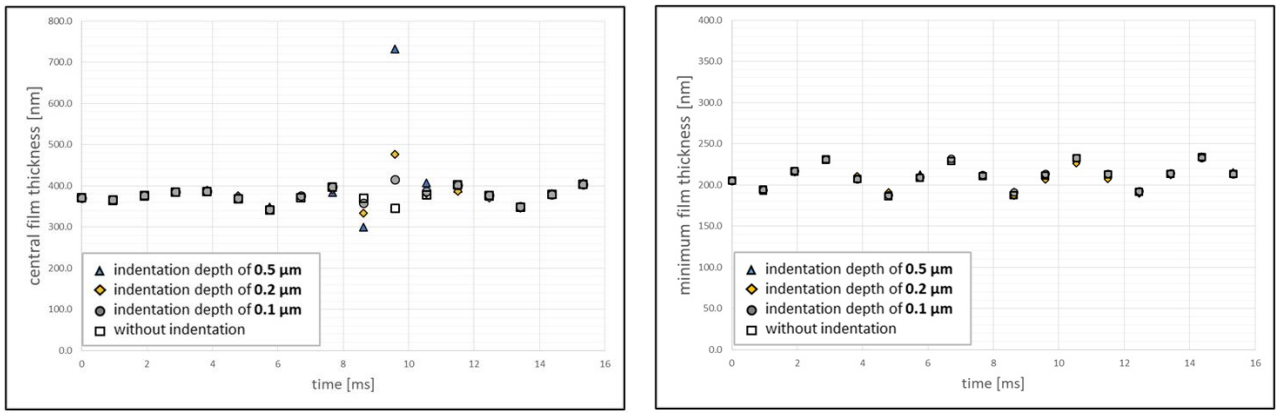

(a) (b)

Fig. 9. Central (a) and minimum (b) film thickness for different depth of indentation

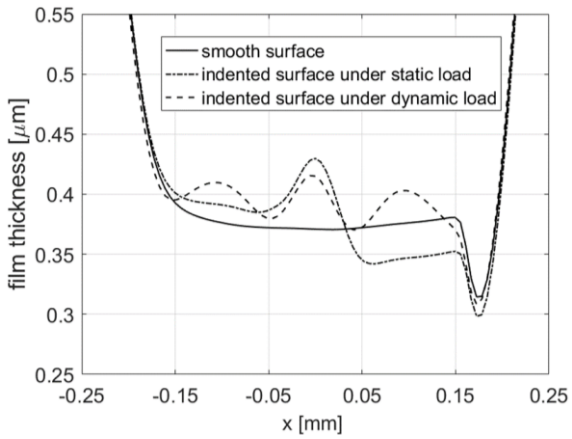

Fig. 10. Film thickness profile for indented surface under static and dynamic load situation. Indentation is momentarily at X_d = 0

4. Conclusions

The numerical analysis for predicting whether an artificial indentation was able to increase lubricant film thickness of a single EHL point contact under dynamic load has been developed in this paper. The following conclusions drawn from the above numerical studies can be summarized as follows

i. The sinusoidal dynamic load caused a harmonic modulation change of the film thickness formation as well as the pressure profile of the contact area, which depended on the frequency and amplitude of the excitation. The frequency excitation impacted the number of modulations of the lubricant film thickness and pressure profile. Additionally, the amplitude directly affected the value of the film thickness increases or decreases in the contact. These results were in a good agreement with Cann *et al.,* [16].

ii. Indentation induced a significant change of film thickness formation on the location of the indentation, which is dependent on its depth. A deeper indentation caused a higher increase of the film thickness at the center of the indentation. However, since the studies conducted under pure rolling condition (SRR = 0), the increase of the film thickness as well as the drop of the pressure profile occured only at the indentation area. This was similar to the experimental and numerical results for the indentation effects on the film thickness under static loads conducted by previous studies [43,44].

iii. Since the single indentation located at the centerline of the contact and the diameter of the indentation studied in this work is much smaller than the contact radius, the increase of film thickness due to indentation occured only at the central film formation. However, this single indentation did not really affect the minimum film thickness because it is well known that for the case of EHL point contact, the minimum film thickness occurs at each of the two sidelobes, instead of at the centerline as in the EHL line contact problem. In order to increase the minimum film thickness, it is worth to place the indentation away from the centerline to the sides.

Acknowledgement
This research was funded by a grant from Universitas Riau.

References

[1] Lanka, Swetha, Venkata Subrahmanyam Sajja, and Dhaneshwar Prasad. "Non-Newtonian Fluid Film Lubrication of Asymmetric Rollers using Vogel Viscosity-Temperature Relationship." *Journal of Advanced Research in Fluid Mechanics and Thermal Sciences* 110, no. 2 (2023): 32-48. https://doi.org/10.37934/arfmts.110.2.3248
[2] Cupu, Dedi Rosa Putra, and Kahar Osman. "Numerical analysis of the effect of temperature on the pressure and film thickness for line contact elastohydrodynamic lubrication using bio-based oils as lubricants." *Journal of Advanced Research in Fluid Mechanics and Thermal Sciences* 92, no. 1 (2022): 90-104. https://doi.org/10.37934/arfmts.92.1.90104
[3] Dowson, Duncan. *Elasto-hydrodynamic Lubrication: The Fundamentals of Roller and Gear Lubrication*. Pergamon Press, 1966.
[4] Dowson, Duncan, and Gordon Robert Higginson. *Elasto-hydrodynamic Lubrication*. Elsevier, 1977. https://doi.org/10.1016/B978-0-08-021302-6.50012-6
[5] Hamrock, Bernard J., and Duncan Dowson. "Isothermal elastohydrodynamic lubrication of point contacts: Part 1-Theoretical formulation." *Journal of Tribology* 98, no. 2 (1976): 223-228. https://doi.org/10.1115/1.3452801
[6] Hamrock, Bernard J., and Duncan Dowson. "Isothermal elastohydrodynamic lubrication of point contacts: Part II-Ellipticity parameter results." *Journal of Tribology* 98, no. 3 (1976): 375-381. https://doi.org/10.1115/1.3452861
[7] Hamrock, Bernard J., and Duncan Dowson. "Isothermal elastohydrodynamic lubrication of point contacts: part III-fully flooded results." *Journal of Tribology* 99, no. 2 (1977): 264-275. https://doi.org/10.1115/1.3453074
[8] Hamrock, Bernard J., and Duncan Dowson. "Isothermal elastohydrodynamic lubrication of point contacts: Part IV-starvation results." *Journal of Tribology* 99, no. 1 (1977): 15-23. https://doi.org/10.1115/1.3452973
[9] Evans, H. P., and R. W. Snidle. "The elastohydrodynamic lubrication of point contacts at heavy loads." *Proceedings of the Royal Society of London. A. Mathematical and Physical Sciences* 382, no. 1782 (1982): 183-199. https://doi.org/10.1098/rspa.1982.0096
[10] Lubrecht, Antonius Adrianus. "The Numerical Solution of the Elastohydrodynamically Lubiricated Line-and Point-Contact Problem Using Multigrid Techniques." *PhD diss., University of Twente* (1987).
[11] Brandt, Achi, and A. A. Lubrecht. "Multilevel matrix multiplication and fast solution of integral equations." *Journal of Computational Physics* 90, no. 2 (1990): 348-370. https://doi.org/10.1016/0021-9991(90)90171-V
[12] Venner, Cornelishenricus. "Multilevel solution of the EHL line and point contact problems." *PhD diss., University of Twente*, 1991.
[13] Zhu, D. "On some aspects of numerical solutions of thin-film and mixed elastohydrodynamic lubrication." *Proceedings of the Institution of Mechanical Engineers, Part J: Journal of Engineering Tribology* 221, no. 5 (2007): 561-579. https://doi.org/10.1243/13506501JET259
[14] Gohar, R., and A. Cameron. "The mapping of elastohydrodynamic contacts." *Asle Transactions* 10, no. 3 (1967): 215-225. https://doi.org/10.1080/05698196708972181
[15] Koye, K. A., and W. O. Winer. "An experimental evaluation of the Hamrock and Dowson minimum film thickness equation for fully flooded EHD point contacts." *Journal of Tribology* 103, no. 2 (1981): 284-294. https://doi.org/10.1115/1.3251647
[16] Cann, P. M., H. A. Spikes, and J. Hutchinson. "The development of a spacer layer imaging method (SLIM) for mapping elastohydrodynamic contacts." *Tribology Transactions* 39, no. 4 (1996): 915-921. https://doi.org/10.1080/10402009608983612
[17] Wijnant, Ysbrand H. "Contact dynamics in the field of elastohydrodynamic lubrication." *PhD diss., University of Twente*, 1998. https://doi.org/10.1016/S0167-8922(99)80089-3

[18] Tallian, T. E. "Paper 14: Rolling contact failure control through lubrication." In *Proceedings of the Institution of Mechanical Engineers, Conference Proceedings*, vol. 182, no. 1, pp. 205-236. Sage UK: London, England: SAGE Publications, 1967. https://doi.org/10.1243/PIME_CONF_1967_182_019_02
[19] Mourier, Louis, D. Mazuyer, A. A. Lubrecht, and C. Donnet. "Transient increase of film thickness in micro-textured EHL contacts." *Tribology International* 39, no. 12 (2006): 1745-1756. https://doi.org/10.1016/j.triboint.2006.02.037
[20] Křupka, Ivan, and Martin Hartl. "Effect of surface texturing on very thin film EHD lubricated contacts." *Tribology Transactions* 52, no. 1 (2008): 21-28. https://doi.org/10.1080/10402000801911838
[21] Ali, Fadi, Motohiro Kaneta, Ivan Křupka, and Martin Hartl. "Experimental and numerical investigation on the behavior of transverse limited micro-grooves in EHL point contacts." *Tribology International* 84 (2015): 81-89. https://doi.org/10.1016/j.triboint.2014.11.025
[22] Ali, Fadi. "Effect of surface texturing on friction and film thickness under starved lubrication conditions." *PhD diss., Brno University of Technology*, 2015.
[23] Wedeven, L. D., and C. Cusano. "Elastohydrodynamic film thickness measurements of artificially produced surface dents and grooves." *Asle Transactions* 22, no. 4 (1979): 369-381. https://doi.org/10.1080/05698197908982938
[24] Kaneta, M., T. Sakai, and H. Nishikawa. "Optical interferometric observations of the effects of a bump on point contact EHL." *Journal of Tribology* 114, no. 4 (1992): 779-784. https://doi.org/10.1115/1.2920948
[25] Ai, Xiaolan, and Herbert S. Cheng. "The influence of moving dent on point EHL contacts." *Tribology Transactions* 37, no. 2 (1994): 323-335. https://doi.org/10.1080/10402009408983301
[26] Venner, Cornelis H., and A. A. Lubrecht. "Numerical simulation of a transverse ridge in a circular EHL contact under rolling/sliding." *Journal of Tribology* 116, no. 4 (1994): 751-761. https://doi.org/10.1115/1.2927329
[27] Venner, C. H., and A. A. Lubrecht. "Numerical simulation of waviness in a circular EHL contact, under rolling/sliding." In *Tribology Series*, vol. 30, pp. 259-272. Elsevier, 1995. https://doi.org/10.1016/S0167-8922(08)70635-7
[28] Wijnant, Ysbrand H., and Cornelis H. Venner. "Analysis of an EHL circular contact incorporating rolling element vibration." In *Tribology Series*, vol. 32, pp. 445-456. Elsevier, 1997. https://doi.org/10.1016/S0167-8922(08)70472-3
[29] Wijnant, Ysbrand H., Cornelis H. Venner, Roland Larsson, and Patrik Eriksson. "Effects of structural vibrations on the film thickness in an EHL circular contact." *Journal of Tribology* 121, no. 2 (1999): 259-264. https://doi.org/10.1115/1.2833929
[30] El Kilali, T., J. Perret-Liaudet, and D. Mazuyer. "Experimental analysis of a high pressure lubricated contact under dynamic normal excitation force." In *Tribology Series*, vol. 43, pp. 409-418. Elsevier, 2003. https://doi.org/10.1016/S0167-8922(03)80068-8
[31] Sakamoto, M., H. Nishikawa, and M. Kaneta. "Behaviour of point contact EHL films under pulsating loads." In *Tribology Series*, vol. 43, pp. 391-399. Elsevier, 2003. https://doi.org/10.1016/S0167-8922(03)80066-4
[32] Glovnea, Romeo, and Xingnan Zhang. "Elastohydrodynamic films under periodic load variation: an experimental and theoretical approach." *Tribology Letters* 66, no. 3 (2018): 116. https://doi.org/10.1007/s11249-018-1067-1
[33] Hajishafiee, A., A. Kadiric, S. Ioannides, and D. Dini. "A coupled finite-volume CFD solver for two-dimensional elasto-hydrodynamic lubrication problems with particular application to rolling element bearings." *Tribology International* 109 (2017): 258-273. https://doi.org/10.1016/j.triboint.2016.12.046
[34] Ardah, Suhaib, Francisco J. Profito, and Daniele Dini. "An integrated finite volume framework for thermal elasto-hydrodynamic lubrication." *Tribology International* 177 (2023): 107935. https://doi.org/10.1016/j.triboint.2022.107935
[35] Stachowiak, Gwidon, and Andrew W. Batchelor. *Engineering tribology*. Butterworth-heinemann, 2001.
[36] Reynolds, Osborne. "I. On the theory of lubrication and its application to Mr. Beauchamp tower's experiments, including an experimental determination of the viscosity of olive oil." *Proceedings of the Royal Society of London* 40, no. 242-245 (1886): 191-203. https://doi.org/10.1098/rspl.1886.0021
[37] Roelands, C. J. A. "Correlational Aspects of the Viscosity-Temperature-Pressure Relationship of Lubricating Oils, Druk." *PhD diss., Technische Hogeschool Delft, The Netherlands*, 1966.
[38] Coulon, Sandrine, Isabelle Jubault, A. A. Lubrecht, Fabrice Ville, and Philippe Vergne. "Pressure profiles measured within lubricated contacts in presence of dented surfaces. Comparison with numerical models." *Tribology International* 37, no. 2 (2004): 111-117. https://doi.org/10.1016/S0301-679X(03)00041-0
[39] Love, Augustus Edward Hough. "IX. The stress produced in a semi-infinite solid by pressure on part of the boundary." *Philosophical Transactions of the Royal Society of London. Series A, Containing Papers of a Mathematical or Physical Character* 228, no. 659-669 (1929): 377-420. https://doi.org/10.1098/rsta.1929.0009
[40] Venner, Cornelis Henricus, and Antonius Adrianus Lubrecht, eds. *Multi-level methods in lubrication*. Elsevier, 2000.

[41] Cupu, D. R. P., Andreas Stratmann, and Georg Jacobs. "Analysis of transient elastohydrodynamic lubrication of point contact subjected to sinusoidal dynamic loads." In *IOP Conference Series: Materials Science and Engineering*, vol. 539, no. 1, p. 012030. IOP Publishing, 2019. https://doi.org/10.1088/1757-899X/539/1/012030

[42] Morales-Espejel, Guillermo E., and Antonio Gabelli. "The progression of surface rolling contact fatigue damage of rolling bearings with artificial dents." *Tribology Transactions* 58, no. 3 (2015): 418-431. https://doi.org/10.1080/10402004.2014.983251

[43] Wedeven, L. D., and C. Cusano. "Elastohydrodynamic film thickness measurements of artificially produced surface dents and grooves." *Asle Transactions* 22, no. 4 (1979): 369-381. https://doi.org/10.1080/05698197908982938

[44] Ai, Xiaolan, and Herbert S. Cheng. "The influence of moving dent on point EHL contacts." *Tribology Transactions* 37, no. 2 (1994): 323-335. https://doi.org/10.1080/10402009408983301